February 5, 2014

Removing Milky Way from airglow images using Principle Component Analysis

Zhenhua Li
Alan Z Liu
Gulamabas G Sivjee

Journal of Atmospheric and Solar-Terrestrial Physics 110-111 (2014) 50–57

Contents lists available at ScienceDirect

Journal of Atmospheric and Solar-Terrestrial Physics

journal homepage: www.elsevier.com/locate/jastp

Removing Milky Way from airglow images using principal component analysis

Zhenhua Li*, Alan Liu, Gulamabas G. Sivjee

Department of Physical Sciences, Embry-Riddle Aeronautical University, 600 S Clyde Morris Boulevard, Daytona Beach, FL 32114, USA

ARTICLE INFO

Article history:
Received 3 May 2013
Received in revised form
17 January 2014
Accepted 28 January 2014
Available online 5 February 2014

Keywords:
Airglow image
Gravity wave
Image processing
Milky Way

ABSTRACT

Airglow imaging is an effective way to obtain atmospheric gravity wave information in the airglow layers in the upper mesosphere and the lower thermosphere. Airglow images are often contaminated by the Milky Way emission. To extract gravity wave parameters correctly, the Milky Way must be removed. The paper demonstrates that principal component analysis (PCA) can effectively represent the dominant variation patterns of the intensity of airglow images that are associated with the slow moving Milky Way features. Subtracting this PCA reconstructed field reveals gravity waves that are otherwise overwhelmed by the strong spurious waves associated with the Milky Way. Numerical experiments show that nonstationary gravity waves with typical wave amplitudes and persistences are not affected by the PCA removal because the variances contributed by each wave event are much smaller than the ones in the principal components.

1. Introduction

Atmospheric gravity waves play important roles in the dynamics and chemistry in the middle atmosphere and lower thermosphere (MLT). Small-scale, short-period gravity waves contribute the majority of the momentum fluxes in the MLT (Fritts and Alexander, 2003). The observation of atmospheric gravity waves is crucial for characterizing gravity wave parameters and quantifying their momentum deposition in the mean flow. Observing wave characteristics is critical for constraining gravity wave parametrization in general circulation models. The small temporal scales of these waves range from buoyancy period (about 5 min in the MLT) to about half an hour. The horizontal scales of these waves range from tens of kilometers to several hundreds of kilometers. The small spatial and temporal scales of these waves pose a challenge for both simulation and observation. Several airglow layers in the MLT region provide excellent proxies to small-scale, short-period gravity waves, among which the OH airglow emission in the near infrared is the brightest. Ground-based all-sky imaging of OH airglow intensity covers an area of hundreds of kilometers with time resolution of minutes, which is suitable for the observation of short-period, short-scale gravity waves.

Methods have been developed to extract gravity information from airglow images. For a broad band airglow image, stars and the Milky Way also contribute significant amount of light. Stars on airglow images are removed by replacing the large intensity pixels by the median values of neighboring pixels or by edge detecting methods (Tang et al., 2003). The Milky Way on the other hand is difficult to remove because it is a bright patch with complex structure and comparable intensity relative to the background airglow emission. The airglow images contaminated by the Milky Way have to be discarded partially (Suzuki et al., 2009; Li et al., 2011) or examined by human eyes to identify real gravity waves. This hampers the ability to objectively estimate gravity wave parameters. A new method needs to be developed to separate the Milky Way emission from OH airglow perturbation due to gravity waves.

In this paper, we present a method to remove the intensity variations due to slow moving Milky Way based on principal component analysis (PCA). In Section 2, the related works on image processing methods to extract gravity waves from airglow images are briefly introduced. In Section 3, the PCA method to remove the Milky Way is described. In Section 4, the effects of the PCA method on gravity wave parameters are investigated using numerical experiments. In Section 5, the gravity wave parameters obtained with and without PCA are compared to show the advantage of the PCA based method. The airglow images used in Sections 4 and 5 were obtained at the Andes Lidar Observatory (ALO) at Cerro Pachon, Chile (30°S, 71°W), where an airglow

* Corresponding author. Tel.: +1 386 226 6710; fax: +1 386 226 6621.
E-mail address: zhenhua.li@gmail.com (Z. Li).

http://dx.doi.org/10.1016/j.jastp.2014.01.016
1364-6826 © 2014 Elsevier Ltd. All rights reserved.

imager is collocated with a sodium lidar and meteor radar on the Andes Mountains since 2009. In the summary section, we summarize the methodology, its benefits, and caveats.

2. Related works

Because airglow image is an effective way to obtain gravity wave information, techniques have been developed to retrieve wave information from airglow images. One technique presented by Gardner et al. (1996) estimates the azimuthal distribution of the horizontal velocity variance from the azimuthal distribution of the relative airglow intensity. The measured variance distribution is applied in the canonical power-law spectrum model (Fritts and VanZandt, 1993) to estimate the gravity wave momentum fluxes as a function of azimuth angle. This technique requires assumption of the spectral shape and that the variance spectra are separable in azimuth and intrinsic frequency. Besides airglow imager data, this technique also needs high resolution zenith and off-zenith lidar wind data for zonal, meridional and vertical wind variance calculation to derive wave momentum fluxes.

Tang et al. (2005a,b) developed an objective way to identify and extract gravity wave information from airglow images. This method has been successfully applied on airglow images to obtain gravity wave climatology at various sites (Espy et al., 2004; Li et al., 2011). Tang's method will be used to estimate wave parameters in this paper and are summarized in the following:

1. *Preprocessing*: All-sky images need to go through the following steps before time-difference (TD) images are produced for wave detection and parameter estimation:
   - The images are interpolated to a uniform curvilinear grid of data points mapped down on to the Earth's surface assuming an altitude of 87 km (nominal altitude of OH airglow layer) to correct the distortion from the fish-eye lens.
   - Stars are attenuated from the images using an edge-detection-based technique. Only the center part of the images (about 90° field of view (FOV) centered at zenith) is further processed because at the edge the spatial resolution is too coarse for small-scale gravity waves due to the distortion of fish-eye lens.
   - Large-scale horizontal waves/structures that can distort the low wavenumber region of periodogram are eliminated by detrending the data, which involves fitting a plane to the 2-D image data analogous to the background line fit to a time series, and then subtracting the plane from the image.
2. *Doppler-shifting*: Doppler effects due to background wind advection need to be corrected. In order to extract intrinsic phase speed of a gravity wave from the observed wave motion, in situ wind advection needs to be accounted either before or after TD. The upside of correcting the Doppler-shifting before TD is that non-wave patterns moving along with the flow are removed. It also keeps stationary waves which would have been removed if TD is performed before correcting Doppler shifting. Three consecutive images are used to generate two TD images. Before the TD images, the wind velocity when an image is taken is estimated from lidar or radar horizontal wind measurement. Three consecutive images form a group and the second image is treated as the base for calculation. Pixels in the first image are shifted in the wind direction by the distance traveled in the time interval between two images. Pixels in the third image are shifted opposite to the wind direction in the same way.
3. *Spectral analysis*: The cross-periodogram of the two TD images is processed to identify dominant monochromatic wave components. Numerical simulations using synthetic waves were used to determine the threshold of 10%, which renders a high probability of detecting a quasi-monochromatic gravity wave and a negligible probability of incorrectly identifying a noise peak as a wave component (Tang et al., 2005a,b). Thus, spectral peaks with energy larger than 10% of the total spectral energy are considered to be significant waves, which are further processed to estimate horizontal wavenumber, propagation direction, intrinsic phase speed, and wave amplitude. The phase speeds are estimated from the phase progression at the spectral peaks between the two TD images.
   Gravity waves that propagate into the MLT are known to have horizontal wavelengths larger than 10 km (Fritts and Alexander, 2003). The identification of spectral peaks therefore is limited for waves with wavelengths larger than 10 km and smaller than the FOV (Tang et al., 2005b; Li et al., 2011). Prior to momentum flux calculation, vertical wavelength of the dominant wave is calculated using gravity wave dispersion relation to determine whether the wave propagates vertically.
   The horizontal wavenumber provides the information on the horizontal scale of the waves and the orientation of wave fronts, which indicates the wave propagation direction with a 180° ambiguity. This ambiguity can be resolved by comparing the phase progression between two consecutive TD images. Because the time interval between consecutive TD images is shorter than half of the typical buoyancy period at the MLT region (about 5 min, lower limit of gravity wave periods), the phase progression between waves on consecutive TD images must be between 0 and 180°.
4. *Momentum flux estimation*: Momentum flux estimation technique is developed by Swenson and Liu (1998) and Haque and Swenson (1999) that is based on a model (Swenson and Gardner, 1998) relating the measured airglow intensity perturbation to the relative atmospheric density perturbation and consequently to the wave amplitude in wind. Quasi-monochromatic waves can be identified and wave parameters can be extracted from TD image sequences using the objective method proposed by Tang et al. (2005a,b). Momentum fluxes then can be estimated using these wave parameters.

One big obstacle encountered when processing airglow images is the slow-moving Milky Way. The Milky Way emission dominates the variation of intensity on the airglow images when it travels across the field of view. The contamination by the Milky Way is larger in the southern hemisphere where the center part of the Milky Way with higher brightness passes close to the zenith. The intensity variation associated with the Milky Way is at least 10 times larger than a typical gravity wave. It cannot be simply removed by differencing consecutive images either because small shifts and variations in the intensity of the Milky Way between images generate residual intensity patterns that are still much larger than most gravity wave amplitudes. Suzuki et al. (2009) designed a method to exclude the image area affected by the Milky Way. They first identified the Milky Way region by obtaining an average star field according to pixels' positions in the equatorial coordinate system (right ascension and declination). If the pixels inside the Milky Way region after detrending are larger than the mean intensity of the whole image, the pixel count is replaced by the mean. The main downside of the method is that the wave pattern inside the Milky Way region is neglected and wave amplitudes estimated using the whole domain are underestimated. Especially when only the central part of all-sky images is used as in our case, the Milky Way region can cover more than 50% of the domain. There is also dark region (intensity smaller than the mean) inside the Milky Way region that together with the replaced Milky Wave region can cause spurious waves. Techniques need to be developed to separate the Milky Way pattern and

short-period gravity waves in order to obtain gravity wave characteristics and momentum flux climatology.

3. Removing the Milky Way

PCA is a mathematical procedure that conducts an orthogonal transformation to convert a set of observations of variables into a set of linearly uncorrelated variables called principal components. The first principal component accounts for as much of the variability in the data as possible, and each succeeding principal component in turn has the highest variance possible under the constraint that it must be orthogonal to (i.e., uncorrelated with) the preceding components. PCA is usually used to capture the dominant variation patterns in the data and perform dimension reduction.

Since the dominant variation in airglow images is associated with the Milky Way and large scale structure of airglow background, the leading principal components would mainly depict these two factors. Reconstructed field using these components is therefore mainly associated with the Milky Way and background airglow emission. The small scale features in the Milky Way still contributed smaller variance to the total variance. These small features are captured by principle components with small eigenvalues. As the number of principal components used to reconstruct the background increases, the horizontal scales of the remaining Milky Way features become smaller. The number of principal components to be included in the reconstructed background field is determined so that the residual pattern associated with the Milky Way has smaller spatial scale than gravity waves (10 km). In practice the number of principle components is set at 50.

The contribution of variance due to gravity waves on the other hand will not be included in the leading principal components because nonstationary gravity waves in the MLT usually have persistence shorter than half an hour and small amplitudes relative to the Milky Way. Even for wave events that last longer than 1 h, the wave parameters often evolve due to the wave dispersion and the background flow. The variation in intensity due to each quasi-monochromatic gravity wave is much smaller than that introduced by the slow progressing Milky Way. Therefore, the leading principal components capture mainly the variations associated with the Milky Way. Removal of the reconstructed field from the original images effectively removes the Milky Way from the images. The PCA removal technique also can remove stationary mountain waves that last for hours. This is not an issue because the method of analyzing difference images is intended to study short-period nonstationary waves and these stationary waves are not common. There are only a few cases during the 3 year observation period at Cerro Pachon, Chile. They can be addressed separately through case studies.

Before PCA, raw airglow images are preprocessed following the steps described in the previous section. Before conducting Doppler-shifting and spectral analysis, the preprocessed image sequences M are used to obtain principal components through PCA. The reconstructed field R using the leading 50 principal components is subtracted from the raw airglow image sequences. The residual field I_{gw} then is analyzed using the spectral analysis method to get gravity wave parameters. The procedure can be described in detail as follows:

$$M = \begin{pmatrix} I_1, \\ I_2, \\ \vdots \\ I_n \end{pmatrix} \tag{1}$$

where I_j, $j = 1, 2, \ldots n$ is an image vector with dimension of $m \times 1$ representing a preprocessed airglow image, where m is the pixel number. M is a $m \times n$ matrix representing the image sequences, where n is the time index. PCA is performed on M by finding the eigenvalues and eigenvectors of the covariance matrix of M. Each eigenvalue corresponds to the variance explained by each eigenvector or principal component. Corresponding to each principal component, there is a principal component coefficient, a time series, which denotes the time evolution of each principal component. The time series can also be interpreted as the projection of image vector on the principal component (eigenvector). The principal components are ordered by its eigenvalue (variance explained). The reconstructed field $R_{m,n}$ is the product of the leading p principal components $P_{m,p}$ and the corresponding principal component coefficient time series $T_{p,n}$:

$$R_{m,n} = P_{m,p} \times T_{p,n} \tag{2}$$

The residual field, I_{gw}, is obtained by subtracting the PCA reconstructed field from airglow images:

$$I_{gw} = M - R \tag{3}$$

I_{gw} is used to obtain gravity wave parameters through steps 2 and 3 in the previous section. Reconstructed images R capture the most part of the slow-moving large scale features associated with background field and the Milky Way. The left column of Fig. 1 shows the preprocessed OH airglow image sequences, M, every 2 h for the night of June 12–13, 2010 at Cerro Pachon, Chile (30°S, 71°W). The right column of Fig. 1 shows the corresponding reconstructed airglow image sequences, R, using 50 principal components. Reconstructed images capture the most part of the slow moving large scale features associated with star field and the Milky Way. A stationary mountain wave lasts about 2.5 h with prominently large amplitudes (30% of the mean airglow intensity) showing up on the northern portion of the first two images of R since it explains a large fraction of variance. The mountain wave has four ridges with stronger amplitudes in the east. The nonstationary gravity wave features in the raw images are not captured by the PCA reconstructed images. Removing PCA reconstructed field effectively removes the Milky Way and retains the small-scale and short-period perturbations of gravity waves. The TD images using raw images have the dominant spectral component associated with Milky Way. Whereas for TD images with PCA reconstructed field, R, removed, the spectral component is dominated by real gravity waves. Some small scale features due to the Milky Way may remain in the images with R removed. They are smaller than gravity wave scales (> 10 km) and will be ignored by the wave detection algorithm.

4. Impacts on gravity wave extraction

In this section, the impacts of the PCA on the gravity wave parameters extraction are investigated. To investigate the effects on gravity waves due to the PCA, we added artificial gravity waves with known parameters into the PCA reconstructed field R to produce an artificial observation set with realistic star field contamination. Wave parameters are extracted from this synthetic airglow image data after removing the Milky Way with PCA method and compared to the original values. The PCA reconstructed field, R, is extracted from one night of OH airglow observation (June 12–13, 2010 at Cerro Pachon, Chile). The interval between the OH airglow images is 1 min. The number of the quality airglow images for that night is 690. The PCA reconstructed images are representation of the Milky Way field and background OH airglow intensity. Then artificial waves are added to the reconstructed field to generate an image sequence of artificial airglow observation. The wave parameters are typical gravity wave parameters and are listed in Table 1. Waves 1–3

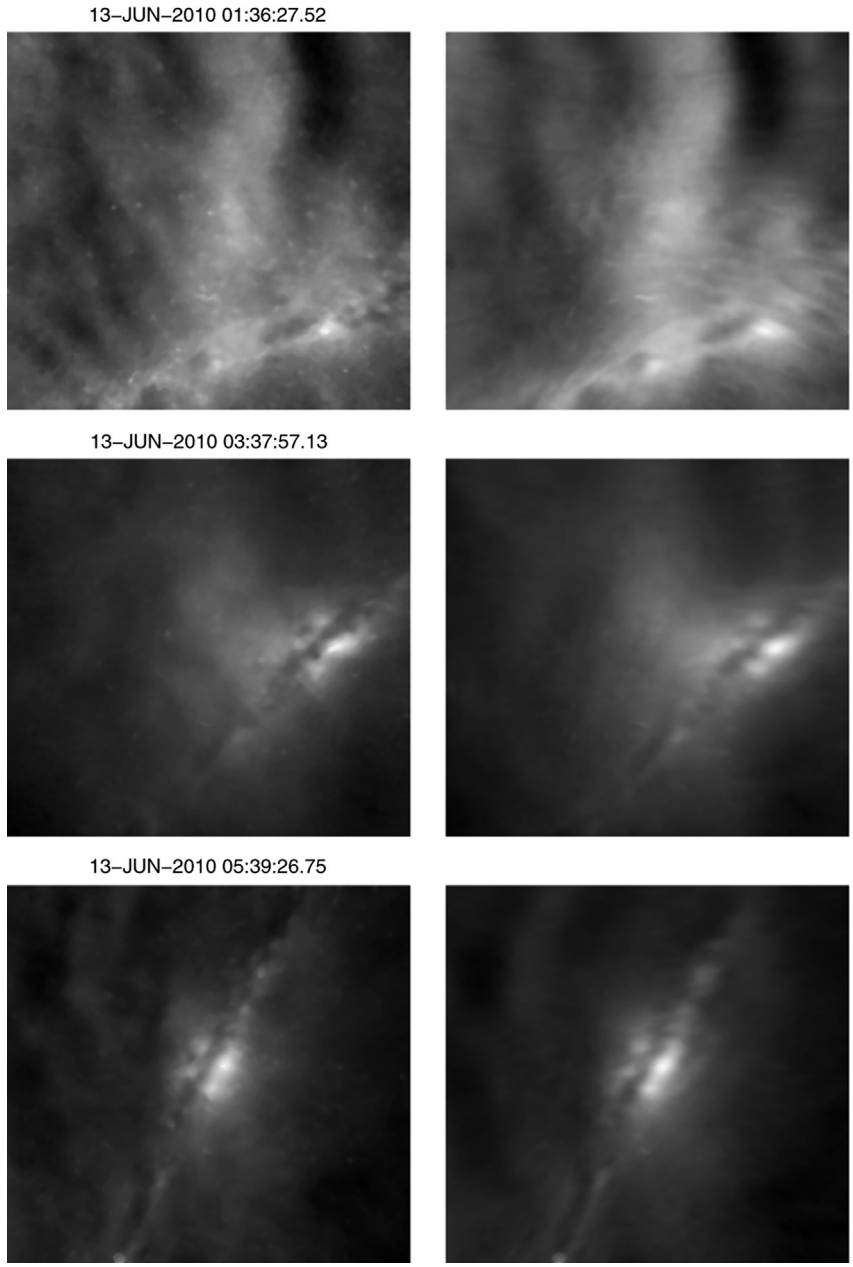

Fig. 1. Raw airglow images (left) and PCA reconstructed images (right) at three times on June 13, separated by 2 h. The time is in UT.

Table 1
Wave parameters of artificial waves and the estimated values with PCA to remove the Milky Way.

Parameters	Waves 1,4	Waves 2,5	Waves 3,6
L_h (km)	20	25	30
Phase speed (ms^{-1})	60	60	60
Experiment 1: Amplitude = 1%			
Estimated			
L_h (km)	19.98	24.96	29.85
Phase speed (ms^{-1})	59.17	59.18	59.01
Amplitude (%)	1.02	0.99	1.00
Experiment 2: Amplitude = 2%			
L_h (km)	19.98	24.97	29.86
Phase speed (ms^{-1})	59.16	59.13	59.61
Amplitude (%)	2.02	1.93	1.92

propagate toward south and Waves 4–6 propagate toward west. Since the majority of waves observed by airglow images have horizontal wavelengths around 20–30 km (Li et al., 2011), the horizontal wavelengths are chosen to be 20 km (Waves 1,4), 25 km (Waves 2,5) and 30 km (Waves 3,6). Phase speeds are set constant at 60 ms^{-1} which is the mean phase speed from previous observations. To investigate the effects of waves with different amplitudes, wave amplitudes are set at 1% and 2% for two experiments which are representative for the majority of gravity waves observed. The wave amplitudes are in percentage of the background airglow intensity. The background airglow intensity is assumed to be 70% of the mean image intensity after the removal of dark counts based on previous measurements at other midlatitude sites (Tang et al., 2005c). Each wave event lasts 30 min which is long enough to represent a typical short-period wave event in the MLT. The background winds are set to constant

at 0 to focus the comparison on the effect of the Milky Way and PCA method.

Then the new image sequences combined with artificial waves and PCA reconstructed field are treated as an observation dataset, M_a. PCA is performed on the synthetic dataset, M_a, to remove the Milky Way and background continuum emission, R_a, and obtain residual with artificial waves, I_{agw}. Then gravity waves are extracted from I_{agw} based on 2-d spectral analysis on Doppler-shifted TD images assuming a uniform background horizontal wind (here, background wind is set to zero) across the image. The retrieved wave parameters as a function of time for the experiment with 2% waves are presented in Fig. 2. Only 2% wave results are shown because estimation errors for 1% waves are even smaller. Larger amplitude waves are more likely to be affected by the PCA removal technique since PCA is designed to identify components that explain the most variances. The results for horizontal wavelengths are almost identical to their original value. Phase speed and wave amplitude show some variability, especially for the larger scale waves. Larger scale waves have fewer cycles in the airglow images, which make phase estimation less accurate. Fig. 3 shows the scatter plot between estimated wave amplitude and wave phase speed for the experiments with 2% wave amplitudes. The high concentration near the fitted slope indicates a high anti-correlation between wave amplitudes and phase speeds. Phase estimation errors in TD images cause wave amplitude errors because wave amplitude estimation is inversely related to phase difference between TD images (Tang et al., 2005b, Eq. (8)). Waves with larger wavelengths tend to have larger errors in phase estimation because they have fewer cycles in the FOV, which in turn causes larger errors in wave amplitude estimation. For an underestimated phase speed, the phase difference between wave components on two consecutive TD images is estimated less than its true value, which can introduce an amplification factor in the amplitude estimation.

Experiments with both wave amplitudes 1% and 2% showed that the PCA method effectively removes the Milky Way and does not affect the extraction of wave parameters. The estimated wave parameters histograms such as wave amplitude and horizontal phase speed for the experiment with amplitude of 2% are shown in Fig. 4. The errors for the experiment with amplitude of 1% are even

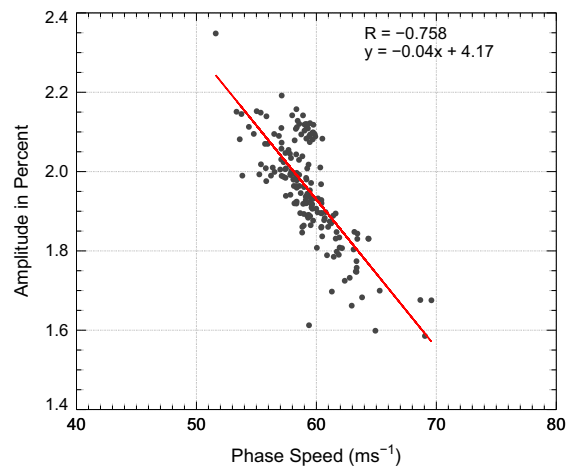

Fig. 3. Scatter plot of estimated phase speed and estimated wave amplitude of the artificial waves in the experiments with 2% amplitudes. The high concentration near the fitted slope indicates a high anti-correlation between wave amplitudes and phase speeds. Phase estimation errors in TD images cause wave amplitude errors because wave amplitude estimation is inversely related to phase difference between TD images.

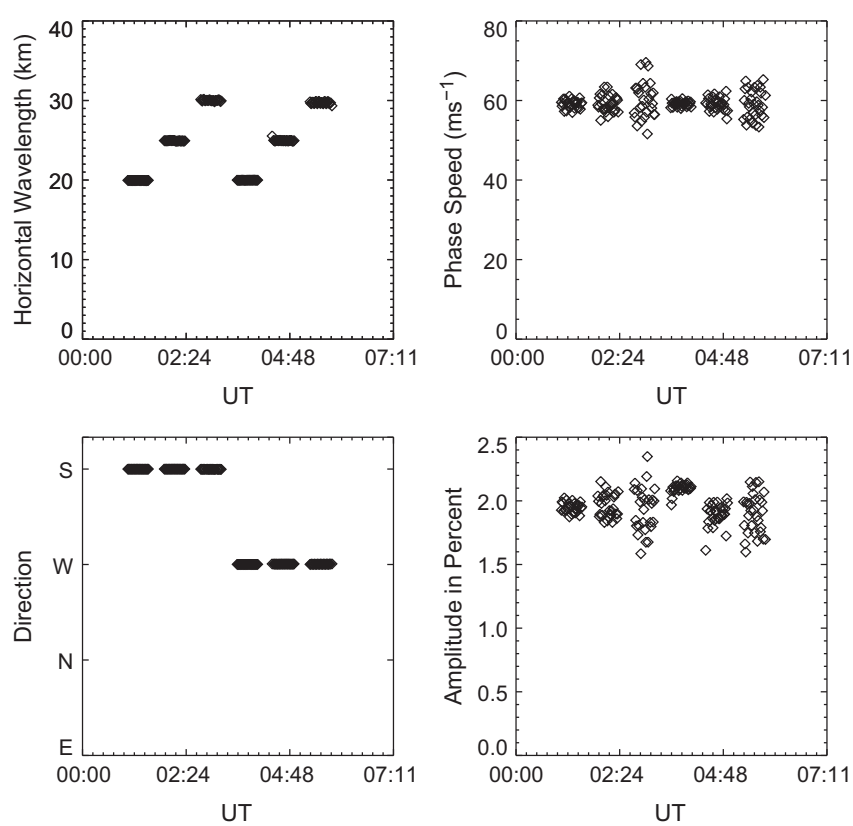

Fig. 2. Wave parameters derived using the method with PCA for waves with wave amplitudes of 2%. The mean values of the wave parameters are very close to their setting parameters. The wave amplitudes and phase speeds for the 30 km waves show larger variability. This is because waves with larger wavelengths tend to have larger errors in phase estimation because of fewer cycles in the FOV, which in turn causes larger errors in wave amplitude estimation.

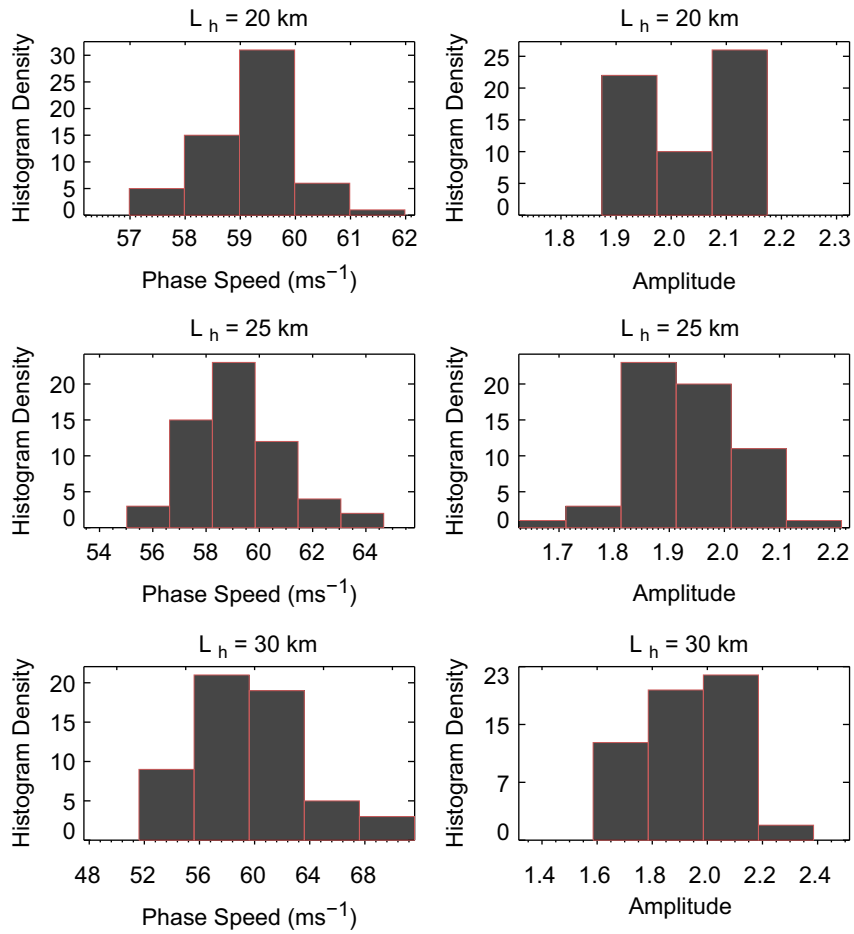

Fig. 4. Histograms of derived wave parameters for artificial waves with wave amplitudes of 2% with different horizontal wavelengths.

smaller. Table 1 shows the mean values for each horizontal wavelength group for the two experiments. The result for large horizontal wavelength waves demonstrates larger variability because there are less cycles in the FOV and the background field contains features of similar scales that are not perfectly captured by R_a. Performing PCA on the synthetic dataset M_a does not remove these few residual features with the new R_a and they remain in I_{agw}. Nevertheless, the mean wave parameters for both experiments are very close to the original ones. They are essentially the same as the original parameters in the artificial waves considering the complex background they are embedded in. This demonstrates that the PCA removal of the Milky Way field does not affect the estimation of gravity wave parameters with moderate amplitudes and normal duration.

5. Comparison using observation

The Milky Way has two effects on gravity wave extraction from airglow images if not treated properly. The first is spurious waves from the pattern associated with the Milky Way. Because of the large amplitudes of these spurious waves, they also make the real gravity waves' signals below the detection threshold (10% of total spectral energy in the FOV). Therefore, in addition to the spurious waves from the Milky Way, the second effect of the Milky Way on wave extraction is to overwhelm gravity wave signal. Even if we can exclude spurious waves based on their propagation direction during the Milky Way's presence, the Milky Way still affects wave parameter extraction by overwhelming gravity wave signal.

To demonstrate the advantage of the PCA methodology, we present here a comparison of wave extraction results using PCA and without PCA on an observation dataset. Among the many differences between the results obtained through these two methods, propagation directions are the easiest to be verified using TD movie. The wave propagation direction statistics are compared in detail for the observation at Cerro Pachon on the night of June 12–13, 2010.

Fig. 5 shows the comparison of the gravity wave propagation direction histogram with PCA and without PCA. The color shading on each pedal represents the phase speed distribution in that direction section. The main feature in the result without PCA is that waves are mainly in the direction of the orientation of the Milky Way. Through the examination of TD image sequences, these waves are identified as spurious waves caused by the Milky Way. Except the propagation direction, the phase speed, horizontal scales of these spurious waves all fall into the reasonable range of gravity waves and are not a unique or constant number. Therefore, it is difficult to discern these spurious waves from real waves without examining the TD movie. The result with PCA shows that the dominant wave propagation direction is between 10 and 30° counterclockwise from east and does not have many waves in the direction of the Milky Way progression. This is consistent with the dominant wave propagation direction from the TD movie.

In Fig. 6, the wave propagation directions as a function of time are plotted for the method with and without PCA. The result without PCA shows persistent wave propagation in the direction of the Milky Way progression (120–150° counterclockwise from the east) between 2 and 8 UT, which are spurious waves. Showing the second effect of the Milky Way, the result without PCA misses

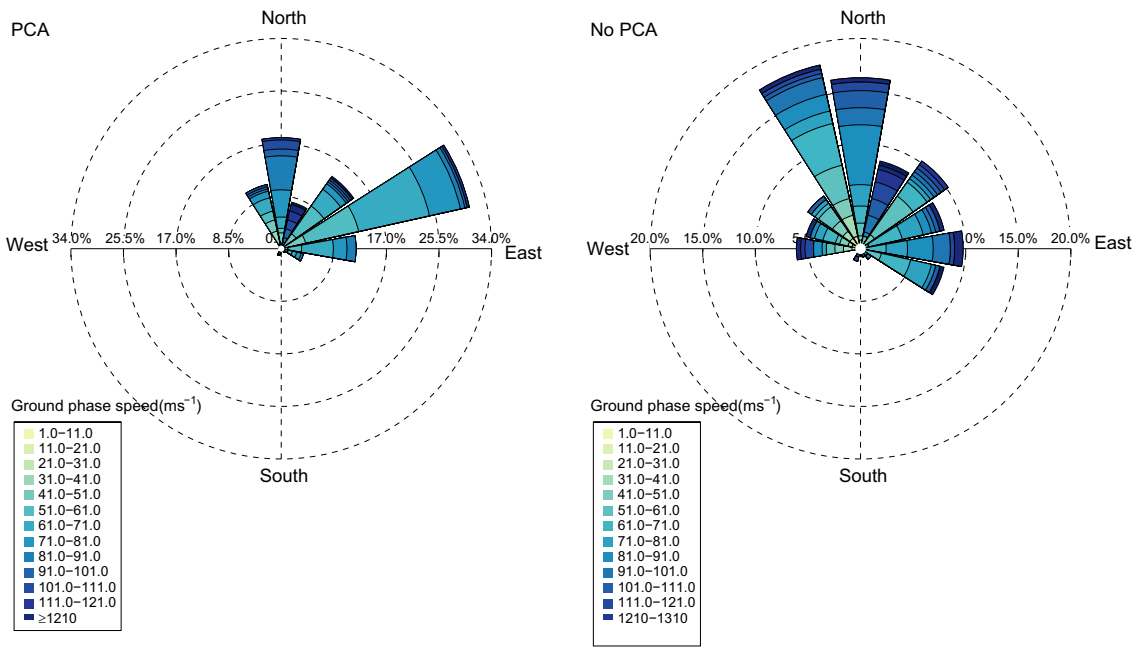

Fig. 5. Propagation direction of gravity waves extracted using the method with PCA (left) and without PCA (right). The color shading denotes ground phase speed distribution in each section. The results without PCA are predominantly toward northwest. The results with PCA are mainly toward northeast which is consistent with TD movie. (For interpretation of the references to color in this figure caption, the reader is referred to the web version of this paper.)

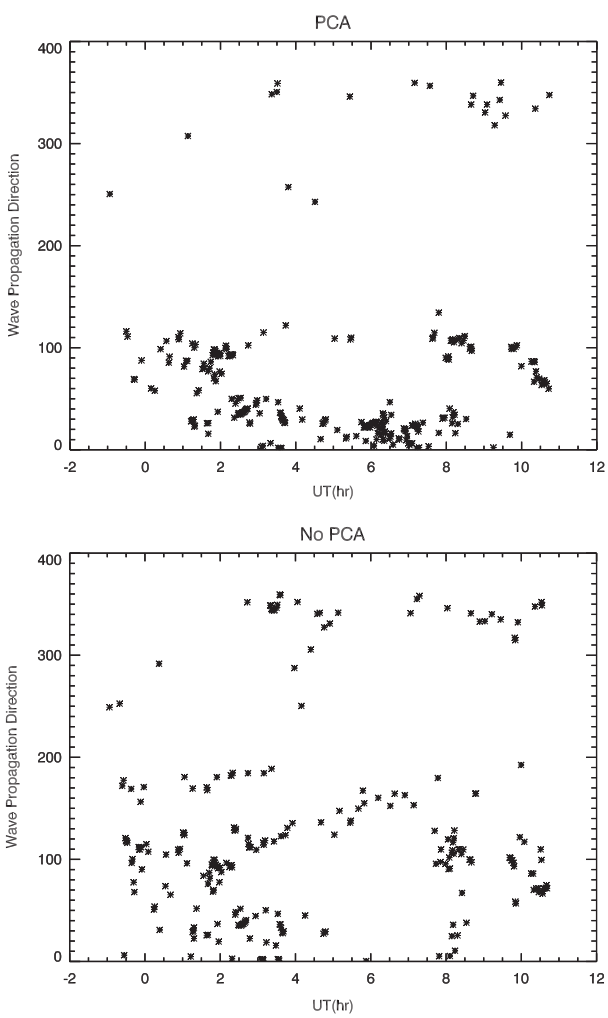

waves propagated toward northeast (about 20–30° counterclockwise from the east) between 5 and 8 UT that are captured by the PCA method and the TD movie. The results with PCA between 5 and 8 UT show that the dominant wave propagation direction is in the northeast (about 20–30° counterclockwise from the east), which matches what is seen from the TD movie. The PCA method effectively removes the spurious waves associated with the Milky Way and gravity wave signals otherwise overwhelmed by the spurious waves can be detected.

6. Conclusion

The Milky Way affects wave parameter extraction by causing spurious waves and overwhelming gravity wave signal. The PCA method effectively removes the effects of the Milky Way on gravity wave extraction from airglow images. The spurious waves from the Milky Way are removed and real gravity waves otherwise overwhelmed by the spurious waves can be detected. The effects of PCA on wave parameter extraction are investigated by numerical experiments. The experiments show wave parameters such as wave amplitudes, phase speeds, and horizontal wavelengths are not affected by the PCA method for waves with normal duration (shorter than half an hour) and amplitudes (about 1–2% of background airglow integrated intensity). Strong and long lasting waves such as orographic waves, however, are removed or attenuated with PCA reconstructed field because their large contribution to the total variance. Long lasting and large amplitude events are not common and can be processed through case studies. The PCA method is nevertheless effective and suitable to extract nonstationary gravity waves from the airglow images with the presence of the Milky Way.

Fig. 6. Time series of propagation direction for the method with PCA (top) and without PCA (bottom). Between 5 and 8 UT, there are many waves propagating toward east for the method with PCA, which can be seen on TD airglow image movie. These waves are absent in the results using the method without PCA.

Acknowledgments

Financial support for this work was provided by the National Science Foundation through Grants number AGS-110199 and AGS-0854704. The former facilitated the operation of the Airglow Imager at the Andes Lidar Observatory in Chile while the latter enabled Polar Airglow Research at the Sondrestromfjord Radar Station in Greenland. We thank Drs. G. Swenson, F. Vargas and A.D. Mangognia from University of Illinois for their assistance in operating the airglow imager at Cerro Pachon in Chile.

References

Espy, P., Jones, G., Swenson, G., Tang, J., Taylor, M., 2004. Seasonal variations of the gravity wave momentum flux in the antarctic mesosphere and lower thermosphere. J. Geophys. Res. 109 (D23), D23109.

Fritts, D.C., Alexander, M.J., 2003. Gravity wave dynamics and effects in the middle atmosphere. Rev. Geophys. 41, 1003.

Fritts, D.C., VanZandt, T., 1993. Spectral estimates of gravity-wave energy and momentum fluxes. 1. Energy-dissipation, acceleration, and constraints. J. Atmos. Sci. 50, 3685–3694.

Gardner, C.S., Coble, M., Papen, G.C., Swenson, G.R., 1996. Observations of the unambiguous 2-dimensional horizontal wave number spectrum of oh intensity-perturbations. Geophys. Res. Lett. 23 (January), 3739.

Haque, R., Swenson, G.R., 1999. Extraction of motion parameters of gravity-wave structures from all-sky OH image sequences. Appl. Opt. 38 (July), 4433–4442.

Li, Z., Liu, A.Z., Lu, X., Swenson, G.R., Franke, S.J., 2011. Gravity wave characteristics from OH airglow imager over Maui. J. Geophys. Res. 116 (November (D22)).

Suzuki, S., Shiokawa, K., Liu, A.Z., Otsuka, Y., Ogawa, T., Nakamura, T., 2009. Characteristics of equatorial gravity waves derived from mesospheric airglow imaging observations. Ann. Geophys. 27 (April (4)), 1625–1629.

Swenson, G., Gardner, C., 1998. Analytical models for the responses of the mesospheric OH* and Na layers to atmospheric gravity waves. J. Geophys. Res. 103 (D6), 6271–6294.

Swenson, G., Liu, A., 1998. A model for calculating acoustic gravity wave energy and momentum flux in the mesosphere from OH airglow. Geophys. Res. Lett. 25 (4), 477–480.

Tang, J., Franke, S., Kamalabadi, F., Swenson, G., 2005a. Motion extraction of atmospheric waves from spectroscopic imaging. IEEE Geosci. Remote Sens. Lett. 2 (2), 229–232.

Tang, J., Kamalabadi, F., Franke, S., Liu, A., Swenson, G., 2005b. Estimation of gravity wave momentum flux with spectroscopic imaging. IEEE Trans. Geosci. Remote Sens. 43 (1), 103–109.

Tang, J., Kamalabadi, F., Rumsey, L., Swenson, G., 2003. Point-source suppression for atmospheric wave extraction from airglow imaging measurements. IEEE Trans. Geosci. Remote Sens. 41 (1), 146–152.

Tang, J., Swenson, G., Liu, A., Kamalabadi, F., 2005c. Observational investigations of gravity wave momentum flux with spectroscopic imaging. J. Geophys. Res. 110 (D9), D09S09.